J. Micromech. Microeng. **19** (2009) 125018 (8pp) doi:10.1088/0960-1317/19/12/125018

Dielectrophoretic deflection of ink jets

Paul R Chiarot and T B Jones

Department of Electrical and Computer Engineering, School of Engineering and Applied Sciences, University of Rochester, Rochester, NY, USA

E-mail: chiarot@ece.rochester.edu

Received 11 June 2009, in final form 8 October 2009
Published 11 November 2009
Online at stacks.iop.org/JMM/19/125018

Abstract

In continuous ink jet systems, streams of ∼10 pL liquid droplets (diameter ∼30 μm) are ejected from an orifice at rates of up to 350 000 per second with velocities in excess of 20 m s^{-1}. Applications as diverse as printing, MEMS fabrication and microarraying benefit from this technology; however, reliable manipulation of the jet, including basic on/off control and steering of the liquid droplets, remains difficult to achieve. We report a novel scheme to manipulate the trajectories of droplets that rebound at shallow angles from a solid substrate using the dielectrophoretic force exerted by patterned electrodes. Varying the voltage applied to the electrodes provides precise control of the rebounding trajectories, mainly by shifting the location of the droplet impact. This technique can also be used to implement on/off control of the droplet stream. A simple dynamic model successfully predicts the modified trajectories of the droplets.

Introduction

A liquid droplet striking a dry solid surface typically exhibits complex flow patterns classified as deposition [1] or splashing [2]. Much of the early effort to understand droplet impact was motivated by applications such as spray cooling, painting and combustion [3]. Under certain conditions, however, a liquid droplet can also bounce or rebound from a solid substrate without breaking up into secondary droplets. Bouncing droplets have been observed on metal surfaces heated above the Leidenfrost temperature [4] and on substrates treated to make them superhydrophobic [5,6]. When droplets rebound they deform, sometimes quite dramatically [7], before recoiling and lifting off the surface. The coefficient of restitution for rebounding droplets can approach unity.

The ability to reflect a liquid droplet controllably from a solid substrate has interesting potential applications in continuous ink jet (CIJ) technologies. In CIJ systems, streams of ∼10 pL droplets (∼30 μm diameter) are ejected from an orifice or an array of orifices at rates of up to 350 000 per second with velocities in excess of 20 m s^{-1}. Applications as diverse as commercial printing, microelectromechanical systems (MEMS) fabrication [8] and microarraying [9] are already associated with CIJ technology or could be exploited. However, reliable manipulation of the stream, including such basic functions as on/off control and steering of the liquid droplets, remains difficult to achieve, especially for the high-density nozzle arrays used in some printers.

In this paper, we report experiments showing that droplet trajectory control can be realized by coupling rebounding droplets with the dielectrophoretic force [10]. This control is achieved by steering the droplets to shift the location of impact along the substrate (figure 1). Trajectory control involves a highly localized, non-uniform electric field near the surface created by patterned electrodes. The resulting non-uniform electric field pulls the droplets toward the substrate, altering the impact point, incident angle and reflected angle of the stream. In this way, we can control the final impact point of droplets on the receiver of the printing system (such as paper or other recording surface). We also describe a second mechanism, not as well understood, that alters the rebound dynamics dramatically to trap the liquid at the substrate and thus provide on/off control.

Although the effect produces a rather modest change in the downstream trajectory, the control of the final droplet position is very precise. This capability facilitates control over jet alignment and should allow for improved resolution in printing and fabrication applications. In the limit of very high electric fields, droplets are trapped at the substrate, making on/off control of the droplet stream possible. One major advantage of using dielectrophoresis (DEP) for trajectory control over traditional electrostatic deflection techniques [11] is that droplet charging is unnecessary, and asynchronous, pulsed or even ac voltage can be used. Furthermore, complex deflection electrode structures are not required. This last

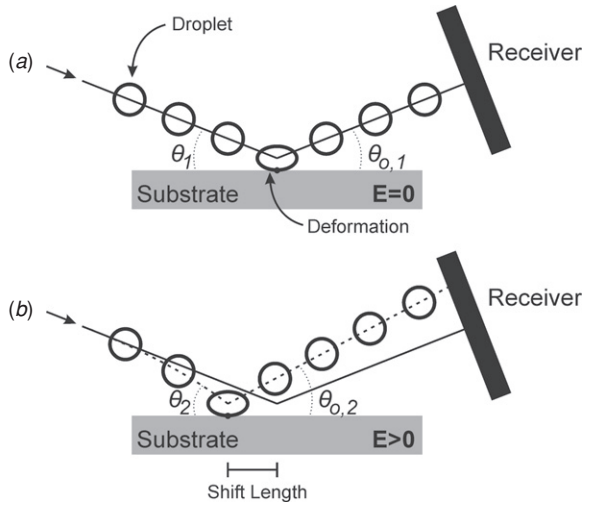

Figure 1. Droplet trajectory control using rebounding droplets and DEP. (*a*) A stream of high velocity liquid droplets is formed and directed toward the substrate where the droplets rebound and continue downstream. Upon impact, the droplets undergo significant deformation. (*b*) An electric field at the substrate surface generates a dielectrophoretic force field on the droplets, modifying the upstream trajectory, shifting the impact point and increasing the incident ($\theta_1 \neq \theta_2$) and reflected angles ($\theta_{o,1} \neq \theta_{o,2}$). This effect changes the downstream trajectory and allows the position of the droplets on the receiver to be precisely controlled by adjusting the voltage. The scale of the image has been exaggerated.

feature is very important in the case of high-density nozzle arrays.

The conditions necessary to achieve reliable droplet rebound and the effect of the dielectrophoretic force on the trajectory are described in the following sections. A simple dynamic model describing the impact behavior is presented which successfully predicts the modified trajectory.

Droplet formation and substrate properties

In all experiments, we used thermal jet nozzle array packages provided by Eastman Kodak Co., Inc. (Rochester, NY) [12]. The nozzles are formed using an integrated CMOS-MEMS process involving deep reactive ion etching to form ~20 μm diameter through holes in a silicon wafer. Metal traces acting as heating elements are also patterned and surround each individual nozzle. The wafers are diced and packaged into standard Pin Grid Array (PGA) chips with a port machined in the underside to allow for fluid connections. A packaged chip is fitted into a PGA socket so that electrical connections can be made to each heating element and an opening at the center of the PGA socket provides access to the port on the back of the PGA chip.

Applying high pressure (~60 psi) to a fluid reservoir upstream from the nozzle produces a cylindrical liquid jet moving at ~20 m s^{-1}. The jet is naturally unstable by the mechanism of the well-known capillary/hydrodynamic instability. To achieve control of the droplet streams, the heating elements surrounding each nozzle are synchronously pulsed to introduce thermal perturbations into the jet. The resulting narrow bands of warmer liquid—just a few degrees

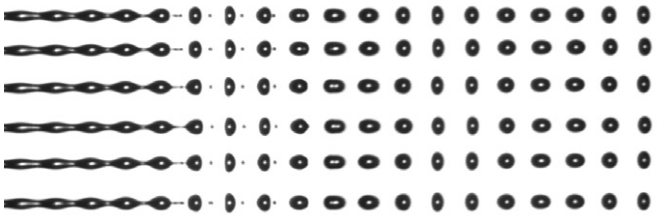

Figure 2. Droplets are formed using a nozzle package provided by Eastman Kodak. The nozzles are located just upstream (left) of the image frame and the droplets are moving from left to right. A regular thermal perturbation provided at the nozzle is used to lock the droplets into a uniform pattern. The liquid jet can be seen collapsing at the centroid of the heat bands. The droplets are travelling at 22.5 m s^{-1} with a spherical size of 33 μm, and each nozzle is producing droplets at a frequency of 310 kHz. The image is captured using a strobe light to fix the droplets in place.

is sufficient—reduce the liquid surface tension locally, which causes the jet to 'pinch off' at the centroid of these heated bands. The frequency of the heating pulses is adjusted to excite the well-known, fastest growing wavelength, which occurs at approximately nine times the radius R of the jet [13]:

$$\lambda \approx 9R. \tag{1}$$

Therefore, for a jet moving at velocity $\mathbf{U}$, if the heaters are pulsed at a frequency of

$$f = \frac{\mathbf{U}}{\lambda} \approx \frac{\mathbf{U}}{9R}, \tag{2}$$

the stream locks into a highly stable, uniform pattern of equal-sized droplets with no satellites. Figure 2 shows a linear array of six droplet streams illuminated by a strobe synchronized to the heating pulse. The 33 μm diameter droplets are traveling at 22.5 m s^{-1} and the heater excitation frequency is 310 kHz. The droplet velocity $\mathbf{U}$ is readily determined using the known strobe frequency and a measurement of the distance between the centers of adjacent droplets. Because there is no mutual coupling, high-density arrays of nozzles can be fabricated and millions of droplet per second can be formed from a very small footprint. In the devices actually used for the experiments reported in this paper, all but one of the nozzles was blocked to facilitate our measurements of droplet trajectory and observations of impact behavior.

The structure used to reflect and manipulate the droplets is a three-layer substrate consisting of a glass slide, a metal layer patterned to form the electrodes and a surface coating. The metal layer is ~100 nm of thermally evaporated aluminum patterned using standard photolithographic methods to form an interdigitated array of coplanar electrodes, as shown in figure 3(*a*). In the experiments, we varied the electrode pitch (w) from ~60 to ~140 μm. The typical overall size of the array is 10 mm wide and 2 mm long. The surface coating is a spin-coated Teflon^{TM} layer with a thickness of 1 μm. Before application of the Teflon, the substrates are treated with fluorosilane to improve adhesion. Doing so extends the life of the coatings from minutes to hours when subjected to the impinging droplet stream.

The high velocity droplet stream is oriented to approach the planar, interdigitated array at a shallow angle (<10°) and

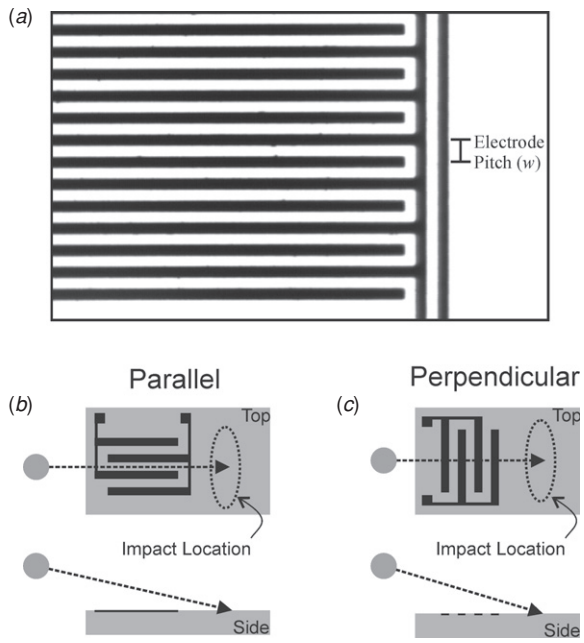

Figure 3. Views of the electrode array. (*a*) Section of the interdigitated electrode array with a center-to-center pitch of 60 μm. The electrodes themselves are 30 μm wide. (*b*) The liquid droplets travel above the array and strike the substrate just beyond the far edge in the impact location. In this case, the stream is oriented parallel to the electrode strips. (*c*) The stream can also be oriented perpendicular to the electrode strips.

to strike the substrate just beyond the far edge of the array (figures 3(*b*) and (*c*)). We perform experiments with the electrode strips of the arrays oriented both parallel and perpendicular to the droplet stream. The width of the arrays is much larger than the droplet size to simplify alignment.

Droplet rebound

Figure 4 shows a stream of water droplets 38 μm in diameter impacting and then rebounding at a shallow angle from a Teflon-coated substrate. Remember that every photo in this study is a compilation of multiple exposures of the droplet stream since the images are captured using a strobe; in the case of figure 4, 1400 exposures are superimposed. During the collision, the droplets flatten into oblate spheroids before recoiling and moving away from the surface. The droplets exhibit some oscillation that appears to die out within $\sim$70 μs after the rebound event. Note that the rebounding droplet shapes suggest a modest amount of rotation, presumably a result of an off-center shear force imparted when the droplet is in contact with the surface.

Before investigating the use of DEP to alter droplet trajectories, it was crucial to determine the conditions necessary to achieve droplet rebound. The ability of a droplet to bounce depends on the properties of the substrate and the Weber number (*We*):

$$We = \frac{\rho \mathrm{U}^2 D}{\gamma} \tag{3}$$

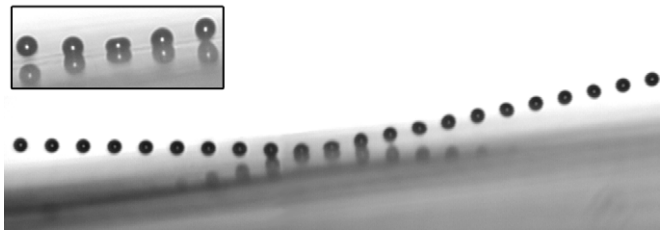

Figure 4. DI water droplets rebounding from a Teflon-coated substrate. The 38 μm droplets are moving left to right in the image with an incoming velocity of 11.5 m s^{-1}. The incident angle is 6.3° and the reflected angle is 6.1°. Inset: zoomed view of the droplets at the point of impact.

with fluid density ρ, droplet velocity $\mathbf{U}$, droplet diameter D and surface tension γ. Consistent with previous experiments on droplet rebound, we find it useful to define a second Weber number, We_n, expressed in terms of $\mathbf{U}_n = \mathbf{U}\sin\theta_1$, the normal component of velocity at the substrate:

$$We_n = \frac{\rho \mathbf{U}_n^2 D}{\gamma}. \tag{4}$$

Sikalo *et al* [14] investigated oblique angle collisions of liquid droplets at solid surfaces and identified an invariant quantity in the form of the normal Weber number, We_n^*, that delineates the boundary between droplet rebound and deposition. In particular, $We_n < We_n^*$ and $We_n > We_n^*$, respectively, for rebound and deposition.

We investigated the impact behavior of water droplets to determine the critical normal Weber number We_n^* for our Teflon-coated substrates. The data plotted in figure 5 delineate the critical regular Weber number (We^*) for which droplet rebound was observed as a function of the incident angle θ_1. The measured values of We^* are converted to We_n^* using θ_1 and the mean of We_n^* is calculated to be $\bar{We}_n^* = 1.09$, a value close to $We_n^* = 1.03$ reported by Sikalo *et al* [14] for water droplets rebounding from a dry, smooth glass substrate. In figure 5, the solid curve represents $\bar{We}_n^* = 1.09$ and it divides the We–θ_1 domain into droplet deposition and droplet rebound regimes. Sikalo *et al* further report a maximum incident angle for rebound of $\sim$7°, the same within measurement uncertainty found in this study. These results indicate that to achieve reliable droplet rebound at a Teflon-coated substrate, the normal Weber number should be less than unity, $We_n < 1$, and the incident angle θ_1 should be less than $\sim$7°. We find that, under these conditions, the uniformity of the reflected droplet stream is maintained many millimeters downstream from the impact point. In the experiments reported in the following sections, these conditions for droplet rebound are maintained when investigating trajectory control using DEP.

Altering droplet trajectory using DEP

The dielectrophoretic force ($\mathbf{F}_{\mathrm{DEP}}$) is effective at moving and manipulating solid particles [10, 15] and liquid droplets or bubbles [16]. Here we exploit $\mathbf{F}_{\mathrm{DEP}}$ to alter the impact and rebound behavior of high-speed droplet streams by creating

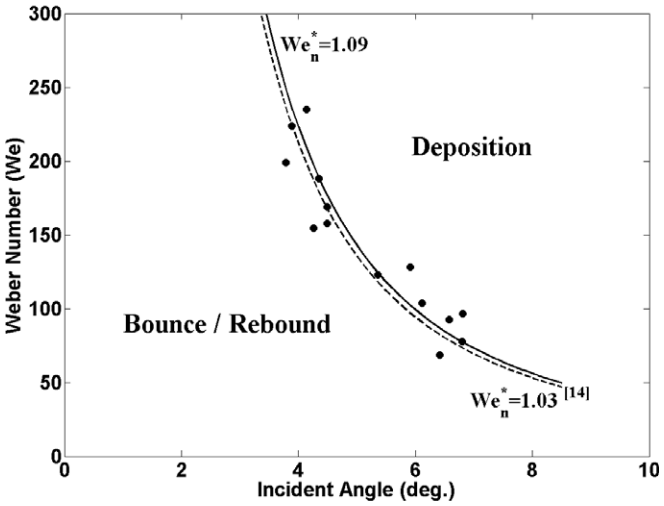

Figure 5. A constant critical normal Weber number (We_n^*) marks the boundary between droplet rebound and droplet deposition. The points represent the measured maximum (i.e. critical) We^* where rebounding occurs for a given incident angle using a Teflon-coated substrate. The solid curve is the mean of We_n^* calculated using the measured data; it is similar to We_n^* reported in [14] shown as the broken curve. The area below the curve is the rebound regime.

a highly localized, non-uniform electric field very close to a substrate surface and then aiming the droplet streams close to the surface. The electric field is created by applying a dc voltage to an interdigitated electrode array embedded in the substrate.

As a droplet travels above the electrode array, the non-uniform electric field pulls it toward the substrate, shifting the point of impact as shown in figure 6. As the voltage is increased, the impact point moves further upstream and the incident angle further increases, though modestly. The effect on the trajectory depends strongly on the distance of the droplet from the surface. The increase in the incident angle is matched by an increase in the reflected angle. The shift of the impact point and attendant increase in the reflected angle are the most obvious measures of the altered downstream trajectory of the droplets.

By shifting the impact point and changing the reflected angle using $\mathbf{F}_{\mathrm{DEP}}$, the downstream position of the liquid droplets (i.e. their location on the receiver) can be manipulated and controlled. The next section presents a simple dynamic model that takes into account the important parameters influencing the trajectory: voltage, electrode pitch, droplet velocity and substrate properties.

Droplet trajectory modeling

Essential geometric parameters for describing the droplet trajectory are shown in figure 7. The rectangular area on the left, designated the *deflection region*, is where the droplet trajectory can be influenced by the non-uniform electric field. It is useful to treat this region as finite in extent, because the electric field and its gradient, strongest close to the electrodes, decay exponentially moving away from the surface. At a distance of $\sim 2w$, the dielectrophoretic force is essentially zero and the effect on trajectory outside this zone is virtually zero. The adjacent, rectangular area at the right, called the *rebound region*, is field-free. Within it, the droplet either rebounds or, if $We_n^* > 1.09$, puddles and forms a rivulet flowing along the surface. The impact shift length $\boldsymbol{L}$ and change of the incident angle $\Delta\theta = \theta_2 - \theta_1$ fully describe the modified trajectory.

The parameter d is the length of the interdigitated electrode array and corresponds to the extent of the deflection region. The parameter c, corresponding to the extent of the rebound region, is the distance from the trailing edge of the

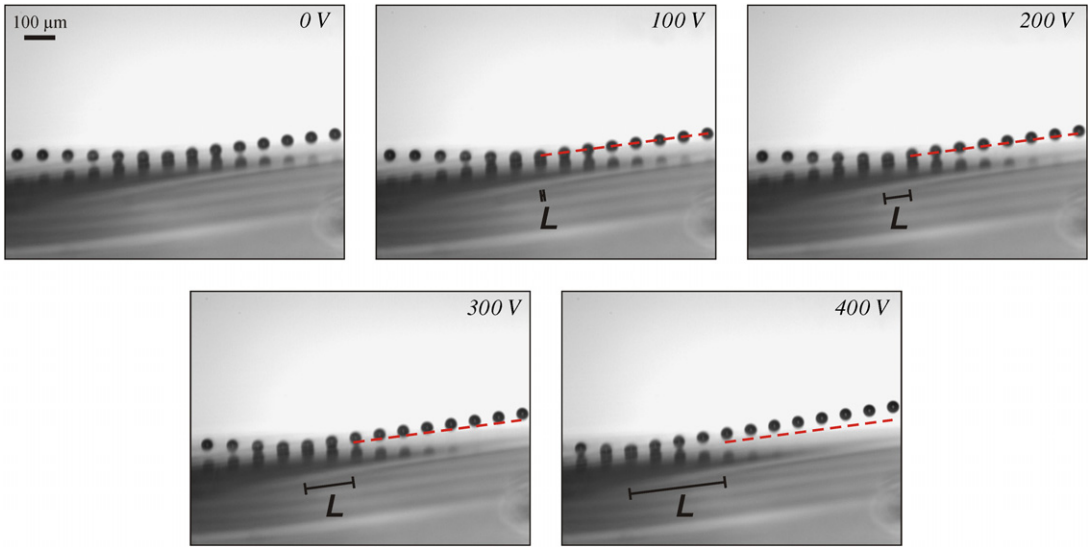

Figure 6. Example of $\mathbf{F}_{\mathrm{DEP}}$ acting on the high velocity droplets. When the dc voltage applied to the electrode array is increased, the point of impact shifts upstream and the incident and reflected angles increase, modifying the downstream trajectory. The broken line is the trajectory of the droplet stream for 0 V and L indicates the shift length compared to the 0 V impact location. The 40 μm droplets are moving left to right in the image.

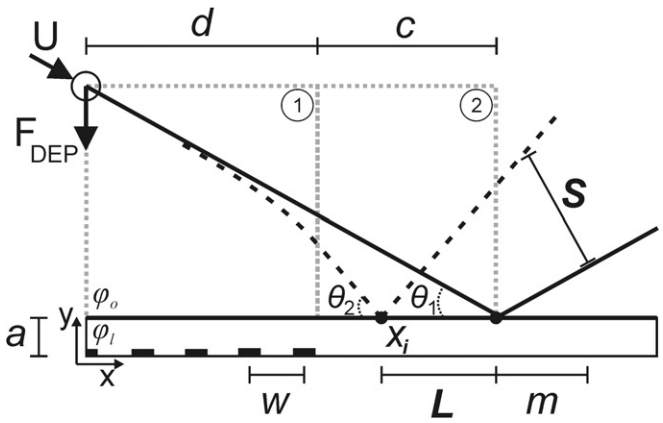

Figure 7. Summary of the problem parameters. The solid line represents the trajectory when $\mathbf{V} = 0$ and the broken line is the modified trajectory. Region 1 is the deflection region above the electrode array and Region 2 is the rebound region. The leading edge of the array is situated at $x = 0$. The scale of the sketch is exaggerated.

array to the point of impact; in this region, $\mathbf{F}_{\mathrm{DEP}} = 0$. The shift length $\boldsymbol{L}$ is measured relative to the point of impact for $\mathbf{V} = 0$. The angle of incidence (θ_1) is determined by finding the angle between lines fitted through the droplet centers and points on the substrate surface when $\mathbf{V} = 0$. The deflection of the droplet stream and position of the droplets at any distance m downstream from the impact point can be conveniently expressed as the parameter $\boldsymbol{S}$:

$$\boldsymbol{S} = \left[\frac{m}{\cos\theta_1} + \frac{\boldsymbol{L}\sin(\pi - \theta_2)}{\sin(\theta_2 - \theta_1)}\right]\tan(\theta_2 - \theta_1). \tag{5}$$

$\boldsymbol{S}$ is the length the reflected droplet stream has shifted perpendicular to the $\mathbf{V} = 0$ case at distance m and it defines the dynamic range of the reflected droplet stream. Its value is determined by the shift length $\boldsymbol{L}$, the trajectory angles θ_1 and θ_2, and the distance m downstream from the original impact point. Note that when calculating $\boldsymbol{S}$, we assume that the incident and reflected angles are equal, which is valid for shallow angle droplet collisions with Teflon-coated substrates.

In the rectangular deflection region, the dielectrophoretic force acts on the liquid droplets, always attracting them downward toward the electrode array. For spherical droplets of radius R, the force is [10, 15]

$$\mathbf{F}_{\mathrm{DEP}} = 2\pi\varepsilon_0 R^3 \nabla E_o^2 \tag{6}$$

with electric field E_o. In equation (6), the Clausius–Mossotti factor is set to unity because the water droplets behave like perfect conductors. To determine an expression for ∇E_o^2 in the deflection region, it is necessary to solve the Laplace equation for the potential field:

$$\nabla^2\varphi = 0. \tag{7}$$

φ_o is the potential field in the deflection region for $y > a$ and φ_l is the potential field in the surface coating layer located between the electrode array and deflection region for $0 < y < a$. Equation (7) is solved analytically using the following boundary conditions:

$$\varphi_l(x, 0) \approx \mathbf{V}\cos(kx) \tag{8}$$

$$\varphi_o(x, \infty) = 0 \tag{9}$$

$$\varphi_l(x, a) = \varphi_o(x, a) \tag{10}$$

$$\kappa\varepsilon_0\frac{\partial\varphi_l(x, a)}{\partial y} = \varepsilon_0\frac{\partial\varphi_o(x, a)}{\partial y} \tag{11}$$

where κ and a are the dielectric constant and thickness of the surface coating, respectively. Equation (8) is a harmonic boundary condition for the periodic electrode array with potential difference $\mathbf{V}$, $k = \pi/w$ and $x = 0$ positioned at the center of an electrode. Note that equation (8) is the first harmonic for the potential with a coefficient that is $\approx 1 \cdot \mathbf{V}$ [17]; higher order harmonics are omitted since their contribution to the potential is small (i.e. coefficients are $\ll 1 \cdot \mathbf{V}$) and they decay rapidly with increasing distance y. Equation (9) means the potential field decays to zero far from the substrate surface and equations (10) and (11) are the continuity conditions at the boundary of the surface coating ($y = a$).

Solving equation (7) for φ_o and φ_l, the potential field in the deflection region ($y > a$) is

$$\varphi_o = \mathbf{V}(1 - \beta + \beta\,\mathrm{e}^{2ka})\,\mathrm{e}^{-ky}\cos kx \tag{12}$$

and the potential field in the surface coating layer ($0 < y < a$) is

$$\varphi_l = \mathbf{V}(\beta\,\mathrm{e}^{ky} + (1 - \beta)\,\mathrm{e}^{-ky})\cos kx \tag{13}$$

where $\beta = (\kappa - 1)/(\kappa - 1 + (1 + \kappa)\,\mathrm{e}^{2ka})$. Note that the factor $(1 - \beta + \beta\,\mathrm{e}^{2ka})$ in equation (12) is due to the influence of the surface coating and it goes to unity when $a \to 0$. E_o^2 in the deflection region ($y > a$) is found by evaluating

$$E_o^2 = \frac{\partial\varphi_o}{\partial x}^2 + \frac{\partial\varphi_o}{\partial y}^2 \tag{14}$$

and the gradient of E_o^2 can then be expressed as

$$\nabla E_o^2 = -2k^3\mathbf{V}^2(1 - \beta + \beta\,\mathrm{e}^{2ka})^2\,\mathrm{e}^{-2ky}. \tag{15}$$

Note that E_o^2 and ∇E_o^2 are functions of y only, the distance normal to the substrate surface, and are independent of x. Thus the dielectrophoretic force is y-directed and constant for a droplet moving tangential to the substrate surface. In fact, for the harmonic field, the magnitude of the dielectrophoretic force is invariant to the electrode orientation (figure 3). Therefore, the orientation of the array can be positioned at any angle relative to the incoming droplet trajectory without changing the expression for ∇E_o^2 or $\mathbf{F}_{\mathrm{DEP}}$.

We find it unnecessary to include higher order multipole correction terms [18] when calculating $\mathbf{F}_{\mathrm{DEP}}$. Their contribution to the force is small because the droplets are always at a distance greater than R from the substrate surface in the deflection region (~1% for the quadrupole when $w = 140\ \mu$m).

By combining equations (6) and (15), $\mathbf{F}_{\mathrm{DEP}}$ is known everywhere in the deflection region. The droplets move with a constant velocity (i.e. the initial velocity) in the x-direction, while the motion in the y-direction is governed by

$$\begin{array}{lll} m\ddot{y} = \mathbf{F}_{\mathrm{DEP}} & \text{for} & x(t) < d \text{ (deflection region)} \\ m\ddot{y} = 0 & \text{for} & x(t) > d \text{ (rebound region)} \end{array} \tag{16}$$

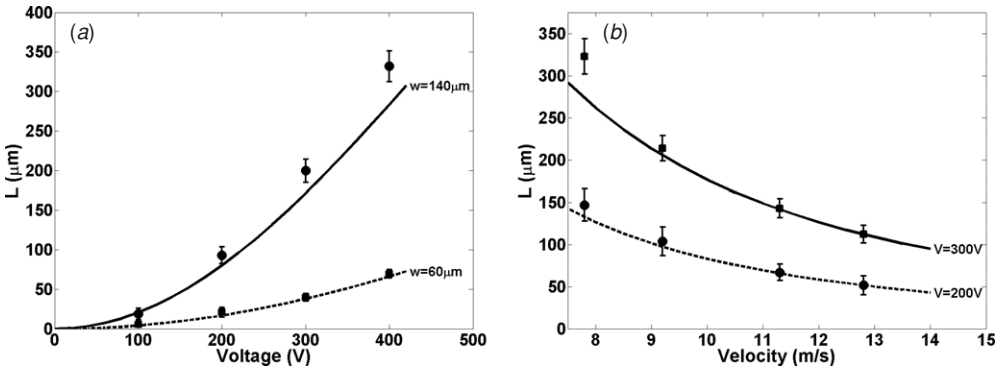

Figure 8. (*a*) Shift length versus voltage for two different electrode pitches with $\theta_1 = 3.9°$, $c = 750$ μm, and $\mathbf{U} = 8.5$ m s^{-1}. (*b*) Shift length versus velocity for two different voltages with $\theta_1 = 3.6°$, $c = 750$ μm, and $w = 140$ μm. The curves are calculated using the trajectory model and the points are the mean of the measured values. The applied voltage, electrode pitch and initial droplet velocity have a significant effect on the shift length and the modified trajectory. The error bars represent the 99% confidence interval for the mean.

where m is the mass of the droplet. The electric field and force on the droplet are assumed to be zero once it is beyond the edge of the electrode array (i.e. no longer in the deflection region); therefore, edge effects have been neglected. Equation (16) is solved using finite differencing with initial position:

$$y(0) = (d + c)\tan\theta_1 + a \tag{17}$$

and initial velocity:

$$v(0) = \mathbf{U}\sin\theta_1 \tag{18}$$

to calculate the trajectory of the droplets. In the rebound region, the droplets move with a constant velocity in both the x- and y-directions. The point x_i is determined for $y(t) = a$ and the shift length $\boldsymbol{L}$ can then be calculated:

$$\boldsymbol{L} = d + c - x_i. \tag{19}$$

In the rebound region the droplet trajectory is linear; therefore, the change in the angle of incidence $\Delta\theta = \theta_2 - \theta_1$ can be easily predicted using the model.

Droplet trajectory results

The curves in figures 8(*a*) and (*b*), predicted using the trajectory model, represent the shift length ($\boldsymbol{L}$) versus voltage ($\mathbf{V}$) for two values of the electrode pitch (w) and shift length ($\boldsymbol{L}$) versus initial velocity ($\mathbf{U}$) for two values of voltage ($\mathbf{V}$), respectively. Measured values of $\boldsymbol{L}$ plotted versus $\mathbf{V}$ and $\mathbf{U}$ show good agreement with these predictions. Error bars on the measured data represent the 99% confidence interval for the mean. The small differences between the measurements and the model are likely a result of three factors: the harmonic assumption for the electric field (equation (8)), the assumption that the field drops to zero immediately at the edge of the array (equation (16)) and uncertainty in the initial angle of incidence (θ_1). The amount of deflection is very sensitive to θ_1; for the case of $w = 140$ μm in figure 8(*a*), reducing θ_1 by 1/10 of a degree in the model will cause a 10% increase in the predicted shift length $\boldsymbol{L}$ at 400 V. Therefore, a very small error when setting θ_1 during testing can lead to significant variations from the predicted droplet deflection.

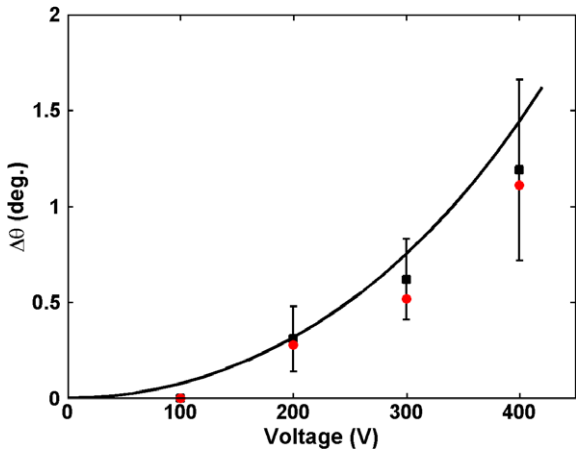

Figure 9. Angle change versus applied voltage for $\theta_1 = 3.9°$, $c = 750$ μm, $w = 140$ μm and $\mathbf{U} = 8.5$ m s^{-1}. The $\Delta\theta$ curve is calculated using the trajectory model and the points are the mean of the measured values for the incident angle (■) and reflected angle (•). The magnitudes of the change in the incident and reflected angle are similar. No change in the angle could be measured for 100 V. Error bars are only shown for the incident angle measurements.

The experiments reveal and the model confirms that the shift length is heavily dependent on the applied voltage ($\mathbf{V}$), geometric parameters (w, θ_1) and the initial droplet velocity ($\mathbf{U}$). The length of the rebound region, c, also has a significant effect on $\boldsymbol{L}$ since it defines the portion of the deflection region that the droplets pass through (i.e. for fixed θ_1, larger c values move the droplet further from the substrate in the deflection region where the field is weaker). Our tests confirm that the orientation of the electrode array with respect to the incoming droplet stream has no effect on the droplet trajectory or the shift length $\boldsymbol{L}$. This result is expected since ∇E_o^2 is only a function of y and therefore invariant to electrode orientation as described in the previous section.

Using the trajectory model, the modified angle of incidence at the point of impact can be predicted and compared to the initial angle of incidence. The predicted and measured change in the incident angle ($\Delta\theta$) versus the applied voltage, along with the measured change in the reflected angle, are shown in figure 9. Though the change in the incident angle

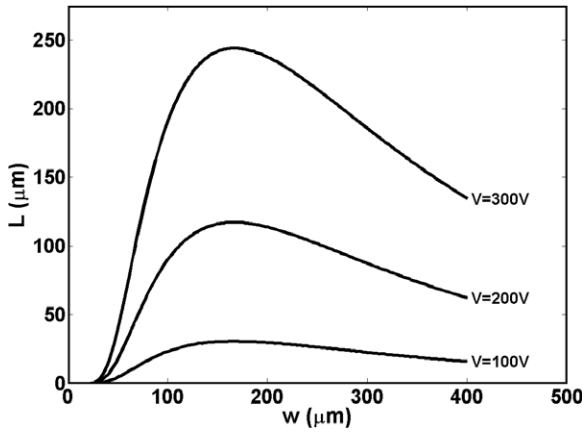

Figure 10. Shift length versus electrode pitch for $\mathbf{U} = 9$ m s^{-1} and $c = 750$ μm. The electrode pitch can be selected (optimized) to maximize the shift length. For typical conditions, the optimized value of w is approximately 160 μm.

($\Delta\theta$) is modest, it translates into an increased reflected angle, thus affecting the downstream trajectory. The magnitude of the change in the reflected angle is the same as $\Delta\theta$ within measurement uncertainty.

Using the shift length $\boldsymbol{L}$ and angle change $\Delta\theta$, the parameter $\boldsymbol{S}$ can be calculated using equation (5). For an incident angle of $\theta_1 = 3.9^\circ$ and electrode pitch of $w = 140$ μm, the shift length $\boldsymbol{L}$ and angle change $\Delta\theta$ are measured to be 332 μm and 1.1°, respectively, for an applied voltage of 400 V. Using these values, at a distance of $m = 1$ mm downstream from the original point of impact, $\boldsymbol{S}$ is calculated to be 48 μm (measured perpendicular to the direction of motion) or approximately 1.25 droplet diameters. The uniformity of the droplet stream persists several millimeters downstream from the impact and $\boldsymbol{S}$ will continue to increase because of the increased reflected angle.

Optimization of electrode pitch (w)

The magnitude of $\mathbf{F}_{\mathrm{DEP}}$ scales as $\mathrm{e}^{-(2\pi/w)y}/w^3$. Smaller values of w create a stronger but more localized force while larger values create a weaker force that extends further out from the substrate surface. Therefore, for fixed c and $\mathbf{U}$, there is a value of w that will maximize the shift length $\boldsymbol{L}$ by optimizing the effective $\mathbf{F}_{\mathrm{DEP}}$ experienced by the droplet during its flight through the deflection region. In figure 10, the shift length $\boldsymbol{L}$ plotted versus the electrode pitch w shows that the optimized value of w is approximately 160 μm when $\mathbf{U} = 9$ m s^{-1} and $c = 750$ μm. Note that changing the values of c and $\mathbf{U}$ will alter the optimized value of w. The curves in figure 10 are calculated using the trajectory model.

Discussion and conclusions

Coupling the rebounding behavior of droplets at a planar surface with the dielectrophoretic force is a novel strategy for droplet trajectory control in CIJ systems. It allows precise control of droplet trajectories using an applied voltage. Because the non-uniform electric field is highly localized and can be changed rapidly by modulating voltage, control of individual droplets with no channel crosstalk should be possible. It is noteworthy that droplet–droplet interactions in CIJ systems are greatly reduced using DEP control instead of traditional charged droplet control since dipole–dipole interactions are of far shorter range than Columbic interactions for equivalent droplet spacing. With individually addressable electrodes, each droplet stream in a high-density nozzle array can be controlled separately if the streams are orientated parallel to the electrode strips (figure 3(*b*)).

The transient response of a spherical droplet to the dielectrophoretic force is governed by the charge relaxation time constant (see Appendix D in [10]):

$$\tau = \frac{\varepsilon_2 + 2\varepsilon_1}{\sigma_2 + 2\sigma_1} \tag{20}$$

where ε_1 and σ_1 are the permittivity and conductivity of air and ε_2 and σ_2 are the permittivity and conductivity of the liquid droplet, respectively. For our experiments, the time constant is $\tau \approx 1$ μs, a full two orders of magnitude smaller than the time spent by a droplet in the deflection region. This is the motivation behind the perfect conductor assumption for the droplets. However, it is noteworthy that because $\varepsilon_2 \gg \varepsilon_1$ and $\sigma_2 \gg \sigma_1$ for droplets in air, the dielectrophoretic force exerted on the droplets will, in fact, be virtually constant for times both shorter and longer than τ. Therefore, it is the electronics that limit the response time of DEP controlled droplet deflection, specifically the rise and fall time of the dc voltage supplied to the electrodes. For our experiments, it is necessary to switch on and off a maximum of 400 V-dc to a purely capacitive load of ~1 pF in a time of the order of ~1 μs. This is not a particularly difficult requirement.

To maintain droplet uniformity, it is best to keep the length of the interdigitated electrode array short ($d = 2$ mm in this study) so that the point of impact can be as close as possible to the nozzle orifice. The highly localized nature of $\mathbf{F}_{\mathrm{DEP}}$ means longer arrays offer no benefit in controlling droplet trajectory anyway, because the gradient of E_o^2 is strong only within a distance of ~w from the substrate surface. The attainable range of final droplet positions on the receiver (defined by the parameter $\boldsymbol{S}$ in figure 7) is limited when using a fixed nozzle. Thus, an ideal implementation would combine DEP control with coarse positioning of the nozzle package, analogous to modern positioning systems that offer high accuracy and large dynamic range.

The shift length $\boldsymbol{L}$ increases directly with voltage; however, there is an upper limit on the maximum allowable voltage where rebound can occur. At sufficiently high voltages, the liquid droplets become trapped in a stream that flows along the substrate. As shown in figure 11(*a*), when $\mathbf{F}_{\mathrm{DEP}}$ becomes sufficiently large to shift the impact point to be atop the electrode array, the impacting droplets collect on the surface and are inhibited from leaving the substrate. In fact, when the impact point is on the array inside the deflection region, the droplets fail to rebound even at moderate voltages; i.e. for $\mathbf{V} < 100$ V as shown in figure 11(*b*). When the voltage is reduced, the downstream droplets freely return to the rebounding condition. This behavior creates an interesting

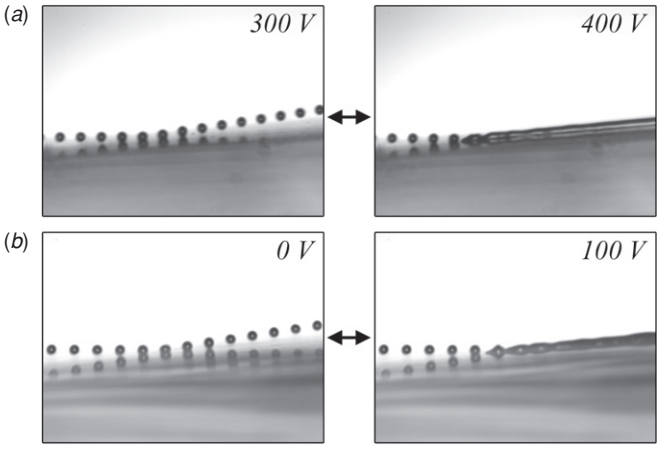

Figure 11. On/off control of the droplet stream. (*a*) For this case at 400 V, the impact location has shifted to be atop the electrode array. When the point of impact is atop the array, the droplets are trapped on the surface and the rebound is suppressed. When the voltage is lowered to 300 V, the downstream droplets return to a rebounding condition. (*b*) When the point of impact is atop the array, the droplets are trapped on the surface even at moderate voltages. Again, when the voltage is lowered, the rebounding condition returns.

possibility for on/off control of the droplet stream in CIJ systems. By correctly positioning the initial point of impact in the rebound region near the trailing edge of the array, it should be possible to combine both trajectory adjustment and on/off control, for example, trajectory control at lower applied voltages and on/off control at a higher voltage.

We have shown that liquid droplets bounce from Teflon-coated substrates when the normal Weber number and incident angle are below certain critical values. The trajectory of the bouncing droplets can be manipulated and controlled by deflecting the droplet stream using the dielectrophoretic force. A simple dynamic model successfully predicts the measured modified trajectory. It was found that the modified downstream position of the droplets was related to the shifting of the impact point and increase in the incident angle. The electrical parameters, specifically the applied voltage and electrode pitch, and the velocity of the droplets, have a significant effect on the magnitude of $\mathbf{F}_{\mathrm{DEP}}$ and shifting of the impact point.

Several important questions are raised by the work presented in this paper, the most important of which concerns the dynamics of droplet trapping on the substrate. The mechanisms involved and conditions required for trapping of the droplet stream are not well understood. Droplets arriving at the surface first spread out and, responding to the applied voltage, flow downstream, apparently contained in a fast-moving rivulet by the very strong, non-uniform electric field created by the strip electrodes. These fluid mechanics, influenced by momentum, surface tension and the liquid dielectrophoretic force, are very complex. Further investigation will require new experiments using a camera of higher spatial and temporal resolution combined with numerical modeling. Other areas for future investigation include the use of new surface coatings to increase the range where bouncing is observed, and the development of novel electrode geometries to further optimize trajectory control.

Acknowledgments

The authors would like to acknowledge Eastman Kodak Co. for their financial and technical support; specifically Justin Gao, Yonglin Xie, Gilbert Hawkins, Ray Yingling and Ali Lopez. They also thank the Center for Electronic Imaging Systems (CEIS) for their financial support. Paul Osborne at the University of Rochester built components for the test fixture used in the experiments.

References

[1] Rioboo R, Marengo M and Tropea C 2002 Time evolution of liquid droplet impact onto solid, dry surfaces *Exp. Fluids* **33** 112–24
[2] Bussmann M, Chandra S and Mostaghimi J 2000 Modeling the splash of a droplet impacting a solid surface *Phys. Fluids* **12** 3121–32
[3] Yarin A 2006 Drop impact dynamics: splashing, spreading, receding, bouncing . . . *Ann. Rev. Fluid Mech.* **38** 159–92
[4] Anders K, Roth N and Frohn A 1993 The velocity change of ethanol droplets during collision with a wall analysed by image processing *Exp. Fluids* **15** 91–6
[5] Richard D and Quere D 2000 Bouncing water drops *Europhys. Lett.* **50** 769–75
[6] Richard D, Clanet C and Quere D 2002 Surface phenomena: contact time of a bouncing drop *Nature* **417** 811
[7] Clanet C, Beguin C, Richard D and Quere D 2004 Maximal deformation of an impacting drop *J. Fluid Mech.* **517** 199–208
[8] Sirringhaus H, Kawase T, Friend R, Shimoda T, Inbasekaran M, Wu W and Woo E 2000 High resolution inkjet printing of all-polymer transistor circuits *Science* **290** 2123–6
[9] Hughes T *et al* 2001 Expression profiling using microarrays fabricated by an ink-jet oligonucleotide synthesizer *Nat. Biotechnol.* **19** 342–7
[10] Jones T B 1995 *Electromechanics of Particles* (New York: Cambridge University Press)
[11] Lee E 2003 *Microdrop Generation* (New York: CRC Press)
[12] Chwalek J, Jeanmaire D and Anagnostopoulos C 2000 Continuous ink jet printer with asymmetric heating drop deflection *US Patent* No 6,079,821
[13] Rayleigh L 1878 On the instability of jets *Proc. Lond. Math. Soc.* **10** 4–13
[14] Sikalo S, Tropea C and Ganic E 2005 Impact of droplets onto inclined surfaces *J. Colloid Interface Sci.* **286** 661–9
[15] Pohl H A 1978 *Dielectrophoresis* (Cambridge: Cambridge University Press)
[16] Jones T B and Bliss G W 1977 Bubble dielectrophoresis *J. Appl. Phys.* **48** 1412–7
[17] Morgan H, Izquierdo A, Bakewell D, Green N and Ramos A 2001 The dielectrophoretic and traveling wave forces generated by interdigitated electrode arrays: analytical solution using Fourier series *J. Phys. D: Appl. Phys.* **34** 1553–61
[18] Washizu M and Jones T B 1994 Multipolar dielectrophoretic force calculation *J. Electrostat.* **33** 187–98